AIAA 80-1381R

Laser-Induced Disturbance with Application to a Low Reynolds Number Flow

George Emanuel,* Michael C. Cline,† and Kathleen H. Witte‡
Los Alamos Scientific Laboratory, Los Alamos, N. Mex.

A novel technique is discussed for nearly instantaneous generation of a strong volumetric disturbance in a flow. This technique utilizes the pulsed energy from an excimer laser to photodissociate a seed gas. Under prescribed conditions, the excess energy associated with the photodissociation is sufficient for producing a severe disturbance. Because it is possible to control the strength and shape of the disturbance, laser energy deposition may become an important tool in experimental fluid dynamics. The effect of laser energy deposition on an inviscid and two low Reynolds number, two-dimensional, supersonic flows is analyzed computationally using the full, unsteady Navier-Stokes equations. There are large differences between the inviscid and viscous flows, with the latter cases showing the presence of a normal-oblique, unsteady shock wave system and of several flow separation regions. It requires 5-10 μs for separation to develop, and the separation is associated only with the upstream edge of the disturbance.

Nomenclature

A = cross-sectional area of beam, cm^2
C_v = specific heat of mixture at constant volume, cal/mole-K
E = energy, cal or cal/mole
E_b = bond strength, cal/mole
E_{ch} = chemical exothermicity, cal/mole
f_p = fraction photodissociated
I = laser intensity, W/cm^2
ℓ = length of excitation volume, cm
M = Mach number
N = number density, cm^{-3}
N_A = Avogadro's number, 6.02×10^{23}/mole
p = pressure, kPa
R = gas constant, 8.314×10^3 kPa-cm^3/mole-K
$\tilde{R}$ = gas constant, 1.987 cal/mole-K
T = temperature, K
V = volume, cm^3
W = mixture molecular weight, g/mole
X = mole fraction
γ = ratio of specific heats for mixture
$\Delta( )$ = jump condition, $( )_2 - ( )_1$
λ = laser wavelength, nm
ρ = density, g/cm^3
σ = photodissociation cross section, cm^2

Subscripts

s = seed gas
u = ultraviolet radiation
0 = stagnation condition
1 = conditions before dissociation
2 = conditions immediately after dissociation

I. Introduction

SHOCK-wave boundary-layer interaction has been of major experimental and computational interest for many years. This interaction, which can lead to separation, becomes especially complex in an unsteady, low Reynolds number flow. Nevertheless, such a flow is examined with an unsteady Navier-Stokes model.[1] The shock-wave system is assumed to be generated by a novel technique: ultraviolet laser photodissociation of a seed gas in a supersonic flow.

Previous analyses of laser energy deposition in a gaseous medium considered applications such as driving a Stirling engine,[2] rocket propulsion,[3,4] or using an absorbing seed gas to shield a surface.[5] The concept here differs from these in that a controlled volumetric disturbance is produced by the laser instantaneously on a fluid mechanic time scale. The strength of the disturbance can be modulated from weak to intense, while the shape of the disturbance can be tailored to produce complex flow patterns. Hence, the excimer (or CO_2) laser may be capable of generating interactions heretofore not experimentally feasible. The disturbance itself stems from the photon energy which exceeds that needed to rupture the bond, and is often substantial in the ultraviolet region. Section II describes the dynamics of the concept and suggests that the technology for it is at hand.

A key aspect is the recent discovery and development of excimer, or Raman-shifted excimer, lasers[6-8] that can efficiently photodissociate many polyatomic molecules. Lasing can be as high as tens of joules per pulse[8] in the ultraviolet region, say 193 to 400 nm, with a duration of a few nanoseconds.[6] The CO_2 laser can also deposit energy in a flow, but excimer lasers may have a number of advantages, such as a short pulse duration and a favorable wavelength region for efficient photodissociation. A very large fluence is required when a CO_2 laser is used for photodissociation, and this fluence further increases as the pressure increases.[9] In contrast to energy deposition by infrared absorption, uv photodissociation can readily augment the disturbance by means of fast exothermic reactions involving the photofragments. Another difficulty in the 10-μm region is that the absorption cross section can be fluence dependent,[9] thus making difficult uniform energy deposition along a collimated beam. Nevertheless, the formulation in Sec. II is easily modified for infrared excitation.

The concept is computationally examined by instantaneously creating an overpressure in a supersonic flow. Section III describes initial flow conditions and the numerical procedure. Time dependent results are presented in Sec. IV, where emphasis is on boundary-layer shock-wave interaction leading to separation. Section V provides our conclusions.

Received Feb. 4, 1980; revision received June 23, 1980; presented as Paper 80-1381 at the AIAA 13th Fluid and Plasma Dynamics Conference, Snowmass, Colo., July 14-16, 1980. Copyright © American Institute of Aeronautics and Astronautics, Inc., 1980. All rights reserved.

*Professor, Dept. of Aerospace, Mechanical and Nuclear Engineering, University of Oklahoma, Norman, Okla. Associate Fellow AIAA.

†Group T-3 Staff Member. Member AIAA.

‡Group C-3 Staff Member.

II. Dynamics of Initial Disturbance

A. Introductory Remarks

A seed gas with mole fraction X_s is assumed to photodissociate in the uv region accessible to excimer lasers. A possible candidate molecule is SF_4. (This candidate is not necessarily a best choice.) The laser wavelength is λ_u, and E_b is the strength of the ruptured bond, e.g., the S-F bond in SF_4. In uv photodissociation the absorbed photon generally exceeds the bond strength in energy, with the difference going into translational and internal excitation. Rapid relaxation of the bulk of the excess energy, on a sub-microsecond time scale, is a consequence of most of the energy appearing as translational energy of the photofragments.[10] On the other hand, for supersonic speeds (e.g., 10^5 cm/s) and a characteristic length of 1 cm, the convection time is of the order of 10 μs. If H_2 is also present, a fast reaction

$$F + H_2 \rightarrow HF + H \tag{1}$$

occurs with exothermicity $E_{ch} = 3.16 \times 10^4$ cal/mole. Reaction (1) is recognized as the pumping reaction for the HF chemical laser. The excess energy

$$E_s = (2.859 \times 10^7/\lambda_u) - E_b + E_{ch} \tag{2}$$

thus heats the gas in a time short relative to convection. (The constant in Eq. (2) converts nm to cal/mole.)

In Sec. B we compute the initial strength of the disturbance associated with E_s. Sections C and D, respectively, evaluate optical thickness and the excitation volume. A summary and several experimental criteria are provided in Sec. E, while Sec. F illustrates the analysis.

B. Strength of Disturbance

Because of the rapidity of the energy deposition, we assume that the density and velocity are initially unaltered. By neglecting the minor change in molecular weight, we have from the equation of state

$$\frac{\Delta p}{p_1} = \frac{\Delta T}{T_1} \tag{3}$$

where Δ denotes the change caused by the energy deposition. Conservation of energy provides

$$\Delta T = (E_s/C_v) f_p X_s \tag{4}$$

where the nomenclature henceforth should be consulted for definitions. Combining the above with

$$C_v = [\tilde{R}/(\gamma - 1)], \quad T_1 = T_0[1 + (\gamma - 1)M_1^2/2]$$

yields for the disturbance strength

$$\Delta p/p_1 = (\gamma - 1)[1 + (\gamma - 1)M_1^2/2](X_s E_s/\tilde{R}T_0) f_p \tag{5}$$

where f_p is evaluated in Sec. IID.

C. Optical Thickness

The change in intensity I for a collimated beam interacting with a medium of length ℓ is given by Beer's law

$$(I/I_0) = \exp(-\ell N_s \sigma_u)$$

With the relations

$$\rho_1 = \rho_0[1 + (\gamma - 1)M_1^2/2]^{-1/(\gamma-1)} \tag{6a}$$

$$\rho_0 = W p_0/RT_0 \tag{6b}$$

we obtain

$$N_s = [1 + (\gamma - 1)M_1^2/2]^{-1/(\gamma-1)} (N_A p_0 X_s/RT_0) \tag{7a}$$

where the number density of the seed gas is

$$N_s = N_A X_s \rho_1/W \tag{7b}$$

For uniform energy deposition, the gas should be optically thin or

$$1 - (I/I_0) < 1 \tag{8}$$

Inequality (8) thus represents a practical limit on ℓ. For simplicity, the use of a reflecting back mirror is not considered, although it would improve uniformity and allow for an increased excitation volume.

D. Excitation Volume and Fraction Photolyzed

The absorbed laser energy is given by

$$\delta E_u = (\rho_1 V_u X_s f_p/W)(2.859 \times 10^7/\lambda_u) \tag{9a}$$

where the factor containing the excitation volume V_u represents the number of moles of seed gas that is photodissociated. By means of Eqs. (6), Eq. (9a) can be written as

$$(\delta E/V)_u = [1 + (\gamma - 1)M_1^2/2]^{-1/(\gamma-1)} \times (p_0 X_s f_p/RT_0)(2.859 \times 10^7/\lambda_u) \tag{9b}$$

To evaluate f_p consider a radiative rate equation for the number density N_s

$$\frac{dN_s}{dt} = -\left(\frac{N_A}{2.859 \times 10^7}\right)(\lambda\sigma)_u I N_s \tag{10}$$

For an optically thin gas, where I is approximately constant along the beam, Eq. (10) can be integrated over the duration of the laser pulse to yield

$$f_p = \frac{(N_s)_1 - (N_s)_2}{(N_s)_1} = 1 - \exp[-(N_A/2.859 \times 10^7)(\lambda\sigma E/A)_u] \tag{11}$$

where E_u is the laser energy, and $(E/A)_u$ is the fluence, given by

$$(E/A)_u = \int_0^{t_{pulse}} I dt \tag{12}$$

E. Summary and Criteria

Equations (2), (5), and (11) provide an estimate for the disturbance strength, which depends on the dimensionless parameters: γ, M_1, $X_s E_s/\tilde{R}T_0$, and f_p. For a strong disturbance, a large value is desired for each of these. A monatomic carrier gas with a low stagnation temperature is thus advantageous. Similarly, the fraction of absorbed energy

$$\left(\frac{\delta E}{E}\right)_u = [1 + (\gamma - 1)M_1^2/2]^{-1/(\gamma-1)} (N_A p_0 X_s/RT_0)\ell\sigma_u \tag{13}$$

should be small compared to unity for nearly uniform energy deposition by a collimated beam. The equations for $\Delta p/p_1$ and $(\delta E/E)_u$ can be viewed as determining ℓ and A_u. The cross-sectional shape need not be circular, e.g., a toroidal cross section can be generated by using an unstable oscillator.

Several criteria are evident, such as an inert carrier gas relative to the seed gas. [For instance, SF_4 rapidly hydrolyzes with H_2O (Ref. 11).] Because of the need for a low stagnation

temperature and high Mach number, both the carrier and seed gases should have adequate vapor pressure for avoidance of condensation. The seed molecule should possess a suitable photodissociation cross section at an accessible uv wavelength with excess energy beyond that needed to break the bond. If necessary, one or both of the photofragments may be used in fast, exothermic reactions.

F. Illustrative Example

We consider a steady, two-dimensional, inviscid nozzle flow with stagnation conditions of 300 K and 0.5 atm. The flow expands to a uniform condition with a temperature of 100 K before dissociation and contains 1.5% of SF_4 seed gas. Two different carrier gases are considered: N_2 ($\gamma = 1.4$), or a monatomic gas ($\gamma = 1.667$). At 100 K the SF_4 has a partial pressure of 0.122 Torr when $\gamma = 1.4$, and 0.366 Torr when $\gamma = 1.667$, while its vapor pressure[11] is 1.5 Torr at 160 K. Thus, the SF_4 is supersaturated at 100 K, but should be able to maintain this state for an adequate period of time, since the supersaturation is not severe.[12] (A condensation criterion is no longer relevant if T_I is increased to about 140 K.)

Unfortunately, there is no published low temperature spectrum of SF_4 in the 190-217 nm region. Bott's room temperature spectrum[13] for the 217-300 nm region shows a sharply increasing continuum cross section below 220 nm. A strong absorption continuum feature, typical of photodissociation, below 220 nm is confirmed by Bott and Jacob's measurements[14] at 235 nm at temperatures near 2000 K. Absorption occurs with a cross section as large as 6×10^{-19} cm^2. As an estimate we use this value for σ_u at 193 nm where the ArF laser operates. Since the S-F bond strength in SF_4 is 78 kcal/mole,[11] E_s is 70 kcal/mole without any chemical augmentation. The photofragments will react, e.g., $2F + M$ and $F + SF_3 + M$ recombination, but these three body, exothermic processes are slow, especially at the elevated temperatures and relatively low pressures that occur after photodissociation, and they can be suppressed with H_2.

The excited volume is assumed to consist of a cylinder with $A_u = 1$ cm^2 and $\ell = 10$ cm. A 4 J (0.956 cal) ArF pulse then produces a disturbance in 10 cm^3 whose strength and absorbed energy are shown in Table 1. The values in the table confirm the possibility of the concept, e.g., $\Delta p/p_I$ is 3.5 with a monatomic diluent. Also shown are the Mach numbers before and after energy deposition. In the monatomic case, the irradiated flow is transonic, while with N_2, conditions correspond to the Sec. IV cases, except for p_0, which is less than 0.5 atm in order to emphasize viscous effects.

In the foregoing a 10 cm^3 volume is used for the irradiation volume. A larger volume, of course, is possible. Its magnitude would depend on the laser's energy, desired disturbance strength, use of a back mirror, etc.

III. Numerical Procedure

We investigate one inviscid and two viscous flows with laser-induced disturbances as computational experiments. A Mach 3 flow in a constant area duct is used that has a half-height of 0.75 cm and is 4 cm in length. This configuration is chosen to illustrate the effects of the laser-induced disturbance and does not correspond to any particular application. Emphasis is on the fluid mechanics of the unsteady duct flow, rather than the steady flow from the upstream supply nozzle.

The flow is calculated with the VNAP code,[1] which solves the two-dimensional, time-dependent, compressible Navier-Stokes equations, and has been used to calculate supersonic as well as subsonic flows.[1,15,16] Interior grid points are computed using the second-order-accurate, MacCormack finite-difference procedure. The no-slip wall and midplane boundary grid points are computed using the MacCormack procedure with one-sided differences normal to the boundary. Supersonic inflow and outflow grid point variables are specified and extrapolated, respectively. Subsonic inflow and outflow as well as free-slip wall boundary grid points are computed using a second-order accurate reference plane characteristic approach. To stabilize the computations for shock waves, an artificial viscosity proportional to the divergence of the velocity is employed. For regions where the divergence of the velocitk is positive (expansions), the artificial viscosity is set equal to zero. This scheme is used in place of the fourth-order smoothing employed by MacCormack,[17] and has been used to calculate shock waves caused by boundary layer separation in supersonic nozzles with good agreement with experiment.[15]

The solution procedure for the inviscid case starts with a uniform, Mach 3 flow of N_2 gas with a total pressure and temperature of 4 kPa (30 Torr) and 300 K, respectively. Laser energy is added to the last 3 cm of the duct by instantaneously raising the pressure and temperature, and the subsequent unsteady flow is computed. At the inflow boundary all variables are specified while at the outflow, where the flow is still supersonic, they are extrapolated.

The viscous cases require specification of the boundary-layer profile at the inflow boundary. For our purposes, the boundary-layer profile could be arbitrarily assumed or calculated from flat plate theory. Instead, we use the VNAP code to generate the boundary layer from a Mach 3 nozzle with a uniform exit core flow, and use the same stagnation conditions and duct size previously discussed. This results in a Reynolds number of 1800 based on the full height of the throat. We thus avoid the complexities of turbulent flow. Low Reynolds number operation also significantly reduces computation time. (The basic concept, clearly, is more general than this restriction.) Velocity and temperature boundary layer profiles at the nozzle's exit constitute inflow conditions for the duct. The duct inflow pressure profile and all profiles outside of the boundary layer are constant. Duct flow, without energy deposition, is computed in time until the boundary layer is steady. Laser energy is then added in the last 3 cm of the duct for the first viscous case, and a 1.5 cm long region in the middle third of the duct for the second case. Finally, the subsequent unsteady flows are computed. There are several grid points, however, in the subsonic part of the boundary layer at the inflow and outflow boundaries that are treated as if this flow is supersonic. Such a procedure produces good results providing the flow is not exiting into a high back pressure region.[15]

The viscous flows use an $81x$ by $41y$ uniform grid for the upper half plane in the duct, and requires 2 min of computation time on the CDC-7600 to reach a physical time of 30 μs.

Table 1 Disturbance characteristics for a 4-J pulse

γ	f_p	$\Delta p/p_I$	$(\delta E/E)_u$	M_I	M_2
1.4	0.903	2.11	0.071	3.16	1.79
1.667	0.903	3.52	0.212	2.45	1.15

IV. Results

When energy is added to the flow, the result is a low-pressure region upstream of a high-pressure region. For the inviscid case, this produces a flow that resembles a shock tube flow with an expansion wave moving downstream relative to the gas, while a shock wave and contact surface move upstream relative to the gas. For the pressure ratio $(p_2/p_I) = 3$ considered here, the upstream velocity of the shock is less than the convection velocity; hence, the shock and contact surface move downstream relative to the duct. Figures 1 and 2 show the pressure and Mach number for the inviscid case, where $t = 0\pm$ denotes conditions just before and after irradiation. Little change occurs with time in the pressure curves except for an increase in the spacing between the expansion and shock, and the increasing width of the expansion. Note that both the downstream facing expansion and the

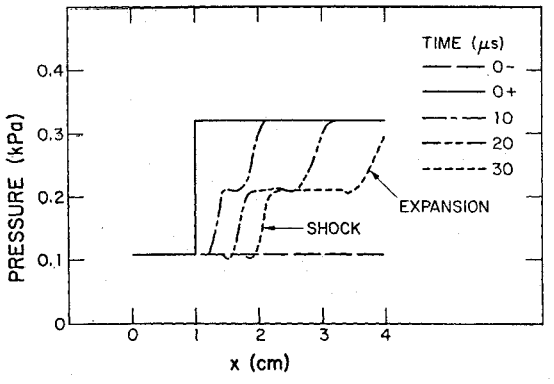

Fig. 1 Inviscid case pressure.

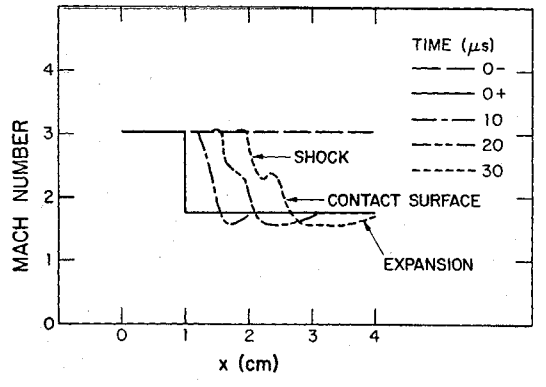

Fig. 2 Inviscid case Mach number.

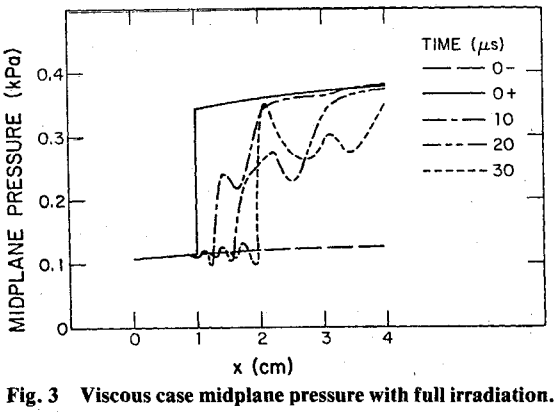

Fig. 3 Viscous case midplane pressure with full irradiation.

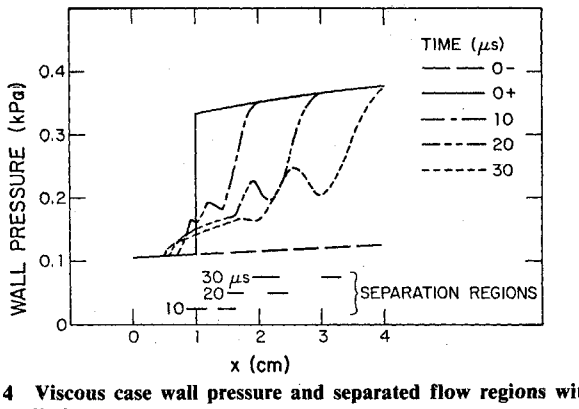

Fig. 4 Viscous case wall pressure and separated flow regions with full irradiation.

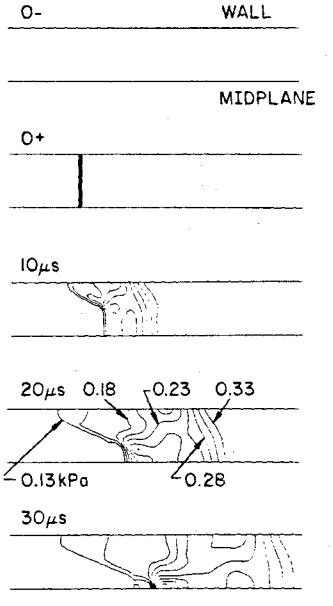

Fig. 5 Pressure contours for viscous case with full irradiation.

upstream facing shock wave produce adverse pressure gradients. The Mach number curves in Fig. 2 show an initial decrease in Mach number due to the shock, a subsequent decrease at the contact surface due to the temperature discontinuity, and finally an increase at the expansion. The contact surface becomes more visible as the spacing between it and the shock increases. The Mach number curves for positive time fall below the $t=0+$ curve because of the upstream particle velocity component produced by the expansion.

In the second case the flow has thick boundary layers. Midplane and wall pressures are shown in Figs. 3 and 4, respectively, while Fig. 4 also shows the regions of boundary-layer separation. Pressure contour plots are shown in Fig. 5, where the top line of each frame is the wall, the bottome line is the midplane, and the flow is from left to right.

In Fig. 3 the $t=0\pm$ pressure curves have a positive slope because of the gradual thickening of the boundary layer in a constant area duct. At 10 and 20 μs the curves resemble the inviscid flow results, whereas the 30 μs curve is different. This difference can be explained by examining Fig. 5, where we see that the high pressure thickens the boundary layer, causing an oblique shock just upstream of the initial irradiation region. (For the extent of the upstream influence, see Fig. 4.) This shock extends downstream joining the core flow normal shock. A second oblique shock is beginning to form at 10 μs that starts at the juncture of the upstream oblique shock and the normal shock and extends downstream to the wall. By 30 μs, the normal shock has vanished and the upstream oblique shock reflects from the duct's midplane. The hump just upstream of the expansion in the wall pressure curves, Fig. 4, is caused by the reflected oblique shock intersecting the wall. The extent of the separated regions at a given time are shown by horizontal lines at the bottom of Fig. 4. The left end of each line represents the separation point, while the right end corresponds to the reattachment point. Hence, there are two distinct separated regions, which correlate with regions of adverse pressure gradient, although these need not occur at the upstream separation points. At 20 and 30 μs the upstream separated region is caused by the reflected shock. By 20 μs, the oblique compression system, upstream of $x=1$ cm, is too diffuse to cause boundary-layer separation. The downstream separated region is caused by the adverse pressure gradient associated with the expansion. The midplane Mach number, Fig. 6, closely resembles the inviscid case results shown in Fig. 2. Mach number contour plots, Fig. 7, also indicate the regions of boundary-layer separation.

Figures 3 and 6 show a numerical oscillation upstream of the shock, which is more severe than in the inviscid case. Both cases use the same artificial viscosity coefficient, $c\Delta x\Delta y\,\rho\,|u_x+v_y|$, where c is a constant, Δx and Δy are the grid

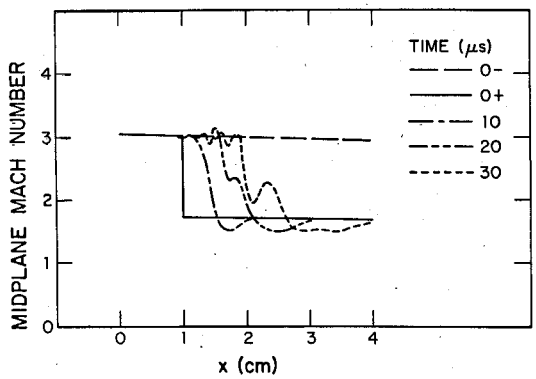

Fig. 6 Viscous case midplane Mach number with full irradiation.

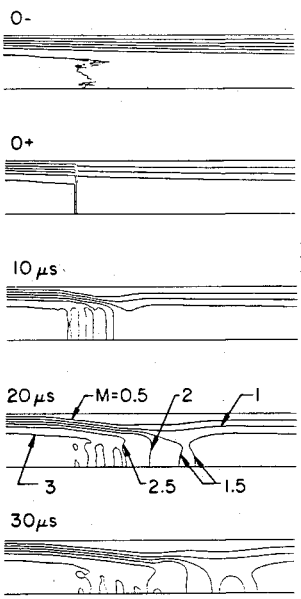

Fig. 7 Mach number contours for viscous case with full irradiation.

spacings, u and v are the velocity components, and the subscripts denote partial differentiation. The viscous case has a Δy that is ¼ the inviscid case value. The artificial viscosity coefficient is therefore smaller for the viscous case. This choice is reasonable because the shock structure in the boundary layer is diffuse. Near the midplane, however, the shocks have the same strength. The smaller artificial viscosity used in the viscous case therefore produces larger oscillations in this small region. Values of c up to eight times the original value reduced the oscillations and spread out the shock waves, but produced no significant change in the overall features of the flow, including the strength of the shocks at midplane, and the separated flow regions.

The last case differs from the second in that the irradiation region has both an upstream and downstream edge. Pressure and Mach number curves, Figs. 8-10, are now for 5, 10, and 15 μs. The upstream part of the midplane pressure curve in Fig. 8 at 10 μs agrees with the 10 μs result in Fig. 3. The downstream part of the pressure curve contains a shock and an expansion, both of which are rapidly moving downstream. Figure 9 shows the expansion wave, which starts at the downstream edge of the irradiation region, propagating upstream in the boundary layer. The separated regions again correlate with regions of adverse pressure gradient. The various disturbances emanating from the downstream edge of the irradiation region, however, produce no separated regions. This is a consequence of the thinning of the boundary layer in this region (see Fig. 11), and the presence of favorable pressure gradients. At 5 μs boundary-layer separation has not occurred anywhere. A finite length of time is required for the development of separation.

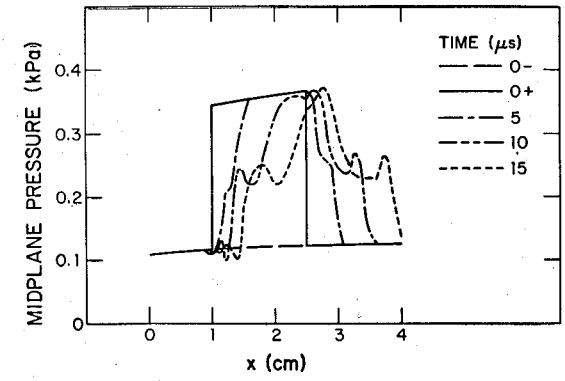

Fig. 8 Viscous case midplane pressure with partial irradiation.

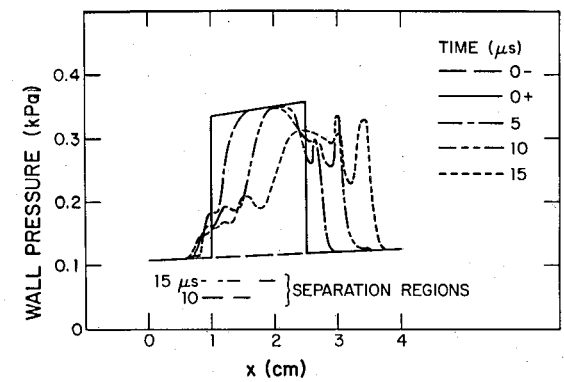

Fig. 9 Viscous case wall pressure and separated flow regions with partial irradiation.

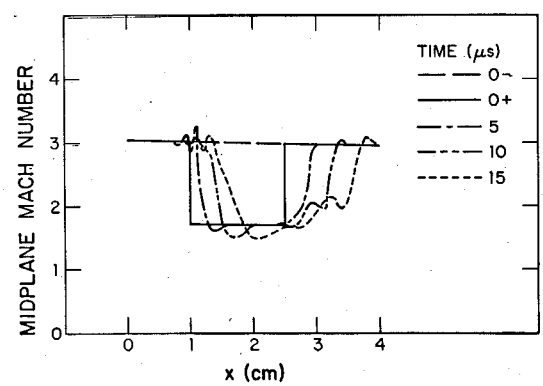

Fig. 10 Viscous case midplane Mach number with partial irradiation.

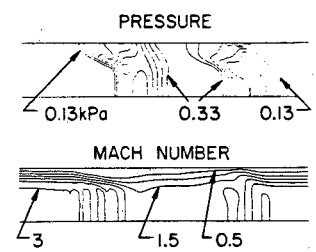

Fig. 11 Mach number and pressure contours for viscous case at 10 μs with partial irradiation.

The upstream part of the midplane Mach number curve at 10 μs, Fig. 10, also agrees with the second case, Fig. 6. Pressure and Mach number contour plots, at 10 μs, are shown in Fig. 11. At the upstream end of the irradiation region, these agree with the 10 μs frames of Figs. 5 and 7, respectively. The favorable pressure gradients at the downstream end of the irradiation region cause considerable thinning of the bound-

ary layer and, therefore, separation does not occur. Note that the downstream shock is not normal to the wall. This shock is propagating into a flow with an established boundary layer, in a fashion analogous to the reflected shock wave in a shock tube flow.

V. Conclusions

The concept is examined of a controlled volumetric disturbance in a supersonic flow caused by means of a seed gas absorbing laser radiation. Key parameters are discussed and we conclude that nearly uniform energy deposition can be obtained sufficient for a large overpressure. By means of an unsteady, Navier-Stokes code, VNAP, three cases are considered. The first is an inviscid flow where the solution is similar to a shock tube flow, but with a uniform convective speed. The remaining cases are viscous. Both exhibit boundary-layer separation, where the separated regions take a few microseconds to develop and then convect downstream. In the first viscous case, the upstream edge of the irradiation zone gives rise to an upstream facing shock wave, a contact surface, and a downstream facing expansion wave. The initially normal shock wave gradually develops into an oblique system of multiple shock waves. The reflected shock and the downstream facing expansion each give rise to a region of separated flow. The last viscous case has both upstream and downstream edges for the irradiation region. For the upstream edge, the resulting flowfield is similar to the foregoing description. While the downstream edge also gives rise to a shock wave, contact surface and expansion fan, none of these features cause boundary-layer separation.

Acknowledgments

The authors are pleased to acknowledge helpful discussions with J. F. Bott. This work was performed under the auspices of U.S. Department of Energy.

References

[1] Cline, M. C., "VNAP: A Computer Program for Computation of Two-Dimensional, Time-Dependent, Compressible, Viscous, Internal Flow," Los Alamos Scientific Laboratory, Los Alamos, N. Mex., Rept. LA-7326, Nov. 1978.

[2] Lee, G., Perry, R. L., and Carney, B., "CO_2 Laser-Driven Stirling Engine," *Journal of Energy*, Vol. 2, July-Aug. 1978, pp. 203-209.

[3] Caledonia, G. E., "Conversion of Laser Energy to Gas Kinetic Energy," *Journal of Energy*, Vol. 1, March-April 1977, pp. 121-124.

[4] Wu, P. K., "Similarity Solution of the Boundary-Layer Equations for Laser Heated Flows," *AIAA Journal*, Vol. 14, Nov. 1976, pp. 1659-1661.

[5] Anderson, J. D. Jr., "Computations of CO_2 Laser Radiation Absorption in SF_6-Air Boundary Layers," *AIAA Journal*, Vol. 12, Nov. 1974, pp. 1527-1533.

[6] Ewing, J. J., "Rare-Gas Halide Lasers," *Physics Today*, May 1978, pp. 32-39.

[7] Huestis, D. L., "The Excimer Age: Lasing with the New Breed," *Optical Spectra*, June 1979, pp. 51-55.

[8] Tisone, G. C., Patterson, E. L., and Rice, J. K., "Studies of an 80-J KrF Oscillator at Excitation Rates of 2-7 MW/cm^3," *Applied Physics Letters*, Vol. 35, Sept. 1979, pp. 437-439.

[9] Ambartzumian, R. V., "Dissociation of Polyatomic Molecules by an Intense Infrared Laser Field," contained in *Tunable Laser and Applications*, edited by A. Mooradian, T. Jaeger, and P. Stokeseth, Springer-Verlag, New York, 1976, pp. 150-161.

[10] Holdy, K. E., Klotz, L. C., and Wilson, K. R., "Molecular Dynamics of Photodissociation: Quasidiatomic Model for ICN*," *Journal of Chemical Physics*, Vol. 52, May 1970, pp. 4588-4599.

[11] Smith, W. C., "The Chemistry of Sulfur Tetrafluoride," *Angewandte Chemie, International Edition in English*, Vol. 1, Sept. 1962, pp. 467-518.

[12] Fisher, S. S., "SF_6 Condensation in Supersonic Nozzle Expansions," *Physics of Fluids*, Vol. 22, July 1979, pp. 1261-1279.

[13] Bott, J. F., private communication of unpublished data.

[14] Bott, J. F., and Jacobs, T. A., "Shock-Tube Studies of Sulfur Hexafluoride," *Journal of Chemical Physics*, Vol. 50, May 1969, pp. 3850-3856.

[15] Cline, M. C., "Computation of Two-Dimensional, Viscous Nozzle Flow," *AIAA Journal*, Vol. 14, March 1976, pp. 295-296.

[16] Cline, M. C., "Stability Aspects of Diverging Subsonic Flow," *AIAA Journal*, Vol. 18, May 1980, pp. 534-539.

[17] Hung, C. M., and MacCormack, R. W., "Numerical Solutions of Supersonic and Hypersonic Laminar Compression Corner Flows," *AIAA Journal*, Vol. 14, April 1976, pp. 475-481.